Supplementary Information

The native oxide skin prevents rapid coalescence of liquid metal Ga nanoparticles during electrocatalysis

Valery Okatenko,[†] Laia Castilla-Amorós,[†] Dragos Stoian,[⊥] Jan Vávra,[†] Anna Loiudice,[†] Raffaella Buonsanti[†]*

[†]Laboratory of Nanochemistry for Energy Research, Institute of Chemical Sciences and Engineering, Ecole Politechnique Fédérale de Lausanne, Sion, CH-1950, Switzerland

[⊥]Swiss-Norwegian Beamlines, European Synchrotron Radiation Facility, 38000 Grenoble, France

*email: raffaella.buonsanti@epfl.ch

Material synthesis.

18 nm Ga NPs were synthesized by modifying a previously reported procedure.[1] 12 mL of ODE and 1.1 mL of DOA were loaded into a 50 mL three-necked flask equipped with a reflux condenser and dried under vacuum at 120 °C for 1 h. Next, the reaction flask was filled with N_2 and heated to 250 °C, followed by a rapid injection of 1.3 mL of *n*-BuLi 2.7 M in a 10 mL syringe. After 30 s, the mixture color changed from colorless to yellow, and 22 mg of $GaCl_3$ dissolved in 0.5 mL of anhydrous toluene were quickly injected with a 2 mL syringe. After that, the heating mantle was removed immediately, and the reaction was quenched with an ice bath after a few seconds after the color changed to dark grey. At 150 °C, 12 mL of anhydrous toluene were injected into the solution, and 0.05 mL of dried OLAC were injected at 50 °C. The solution was then left stirring for a few minutes. To purify Ga NPs and separate them from by-products and unreacted precursors, 15 mL of anhydrous ethanol were added, followed by centrifugation at 5000 rpm for 20 min. After supernatant disposal, the Ga NPs were redispersed in anhydrous toluene, and the purification/precipitation step was repeated once more with addition of 0.1 mL of OLAC. The Ga NPs were finally stored in anhydrous toluene.

39 nm Ga NPs were synthesized by following the same synthetic protocol used for the *26 nm* Ga NPs, except that the precursor solution injected at 290 °C consisted of 40 mg of $Ga_2(NMe_2)_6$ and 3.4 mL of DOA in 2.6 mL of dried ODE.

Ga microparticles (MPs) were synthesized according to Falchevskaya *et al.*[2] In a typical synthesis, 50 mg bulk gallium was placed in a 20 mL glass vial with 10 mL of toluene and heated at 50 °C until the drop melted. The vial was then subject to ultrasound treatment in the ultrasonic bath (Bandelin Sonorex) at 50 °C until the full dispersion of the metal, which took *ca.* 30 min. Upon completion, the Ga MPs were left to cool down and stored in the same vial.

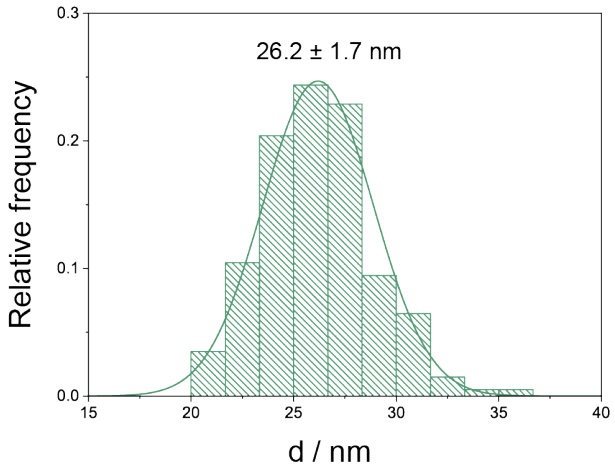

Figure S1. Size distribution of 26 nm Ga NPs.

Surface area calculation. We found that the electrochemical double-layer capacitance or underpotential deposition are not readily accessible to determine the electrochemically surface area (ECSA) for Ga. The use of these methods generates unreliable and irreproducible results. The presence of a native oxide layer in all the voltage ranges where no Faradaic processes occur might explain these issues, which are similar to those encountered for oxide electrocalysts.[3] Impedance measurements with the implementation of equivalent electric circuit have been used for oxide electrocatalysts.[4–6] However, this circuit has to be reliably established first for the given system, which is beyond the scope of this study.

Similarly to Reske et al.,[7] we have defined the total surface area, S (cm^2) as follows:

$$S = S_P N_P = \pi d_p^2 \cdot \frac{m_{total}}{m_p} = \frac{\pi d_p^2 m_{total}}{\rho_{Ga} V_p} = \frac{\pi d_p^2 m_{total}}{\rho_{Ga} \cdot \frac{1}{6}\pi d_p^3} = \frac{6 m_{total}}{\rho_{Ga} d_p},$$

where S_P (m^2) is a surface area of a particle, N_P is a number of particles, d_p (m) is the average particle diameter (obtained from the particles size analysis), m_{total} (kg) is the catalyst loading, m_p (kg) is a particle mass, $\rho_{Ga} = 6095$ kg m^{-3} is the density of liquid Ga,[8] V_p (m^3) is a particle volume.

To transfer to more convenient units with respect to the scale (cm^2, nm, μg, g, cm^3), correction coefficient is needed, and the final formula yields

$$S = \frac{60 m_{total}}{\rho_{Ga} d_p},$$

where the units are S_P (cm^2), m_{total} (μg) is the catalyst loading, ρ_{Ga} (g cm^{-3}), d_p (nm).

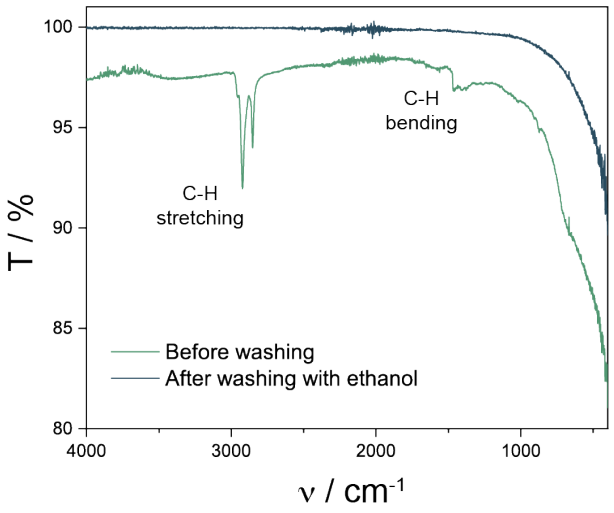

Figure S2. FTIR spectra of Ga NPs drop-casted on glassy carbon before (green curve) and after rinsing the surface with ethanol (black curve). Disappearance of the aliphatic features after ethanol washing indicates removal of the ligands.

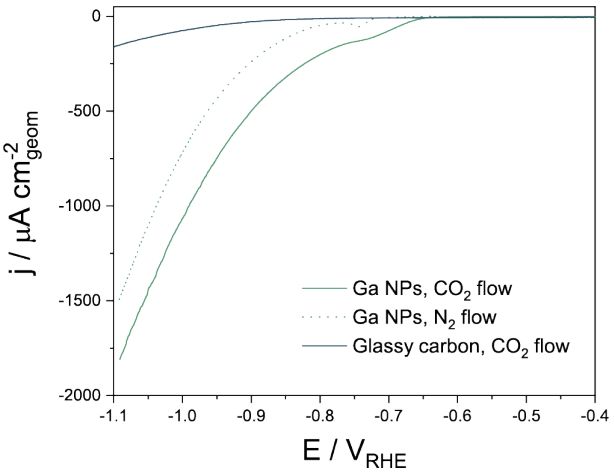

Figure S3. Linear sweep voltammetry of Ga NPs under CO_2 (green curve) and N_2 flow (green dot curve) compared with clean glassy carbon substrate under CO_2 flow (black curve).

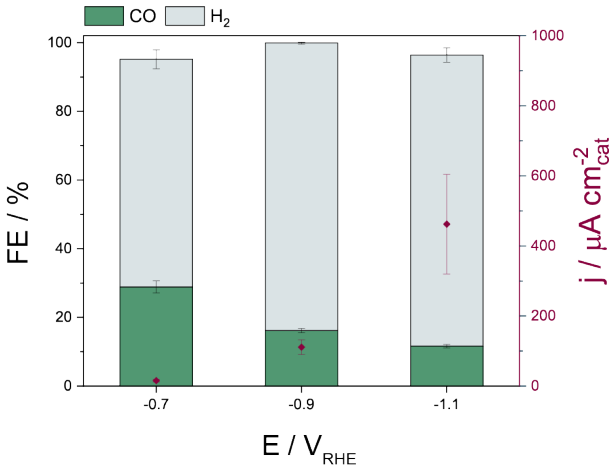

Figure S4. Average CO and H_2 FE and current density for Ga NPs over 1 h CO_2RR at different potential together with the corresponding measured density (j) current reported on the right axis.

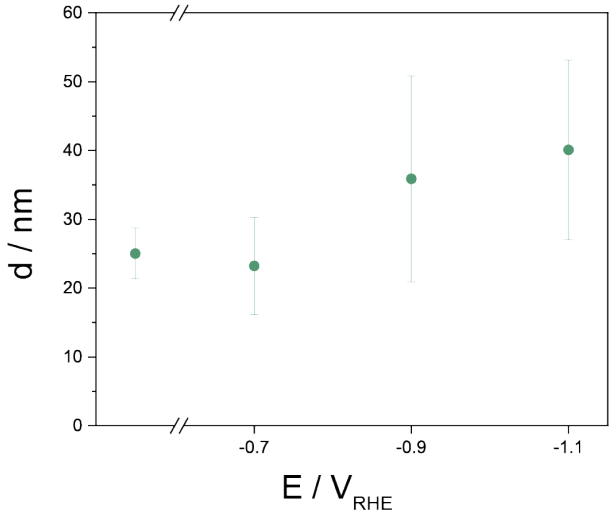

Figure S5. Statistical analysis performed on SEM images of Ga NPs after 1 h electrolysis at different voltages. The first point refers to the size of Ga NPs on the as-prepared electrode. Broader size distribution for pristine Ga NPs compared to the data in **Figure S1** is due to lower resolution of SEM imaging compared to TEM.

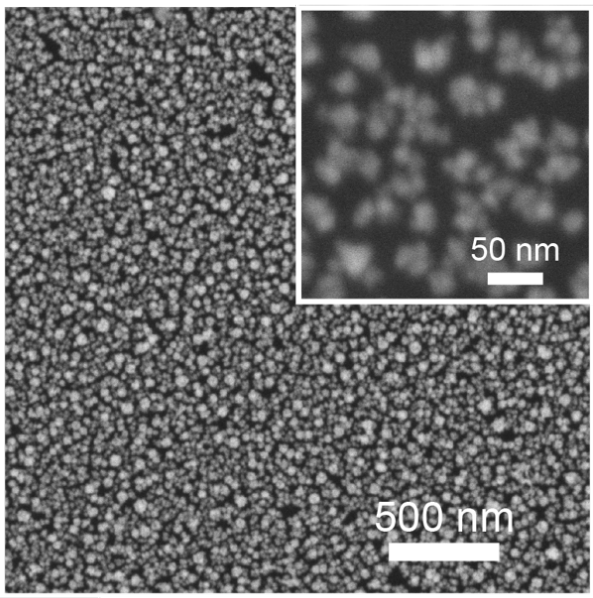

Figure S6. SEM image of Ga NPs electrodes after 70 h electrolysis at -0.7 V_{RHE} in 0.1 M $KHCO_3$.

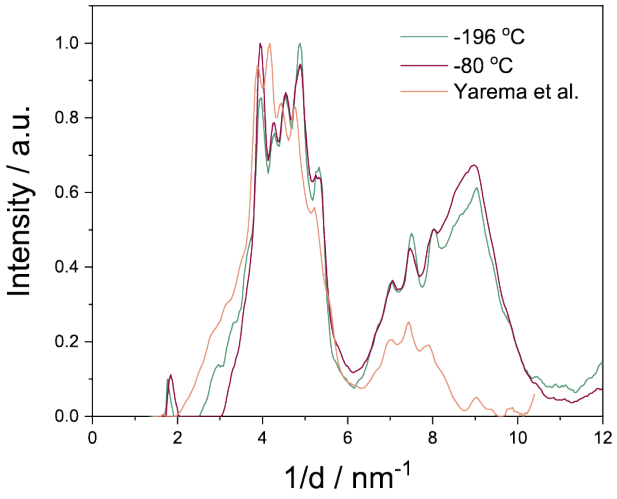

Figure S7. Circular averaged electron diffraction pattern of Ga NPs at -196 °C and -80 °C; for reference, the circular averaged electron diffraction pattern obtained by Yarema et al.[9] is presented.

Gallium oxide shell thickness calculated by XPS measurements.

The Ga-oxide shell thickness (*d*) for the Ga NPs was calculated by using XPS technique following a previously reported procedure.[10] Specifically, *d* is calculated by using the well separated Ga-metal and Ga-oxide peaks in the Ga2*p* region of the XPS spectrum (see **Figure 2**). The following equation describes the relation between *d* and the amount of Ga-oxide measured by XPS:

$$d = -\lambda * \ln\left(\frac{\%Ga_2O_3 - \lambda}{-\lambda}\right)$$

where λ is the inelastic mean free path (Å), and $\%Ga_2O_3$ is the percentage of Ga_2O_3. The λ value was calculated for the Ga2*p* photoelectrons to be 11.3 Å as described by Castilla-Amorós et al.[10] Note that the $\%Ga_2O_3$ values are the area percentages of the oxides obtained from the Ga 2*p* high resolution XPS spectra multiplied by the calculated $\%Ga_2O_3$ to give an area that is compatible with the model as previously reported.[10] This approach provides approximations to the Ga-oxide shell thickness within *ca*. 10%. In particular, the Ga-oxide shell thickness measured after 1 h electrocatalysis carried out at different applied potentials is reported in **Table S1**. No particular trend of the shell thickness versus applied potential is evident. We note that the shell thickness of the as-prepared Ga NPs matches the one measured by TEM and *operando* XAS measurements. Instead, larger shell thickness values compared to the one obtained from operando measurements can be explained by the fact that the Ga NPs are exposed to the electrolyte and air before the XPS measurement is carried out.

Table S1. Ga_2O_3 shell thickness after electrolysis performed at different applied potential as calculated from the XPS data.

Applied potential / V_{RHE}	**Ga_2O_3 shell thickness / nm**
As-prepared Ga NPs	2.7
Ga NPs 1 h @ -0.7 V	2.3
Ga NPs 1 h @ -0.9 V	1.6
Ga NPs 1 h @ -1.1 V	2.0

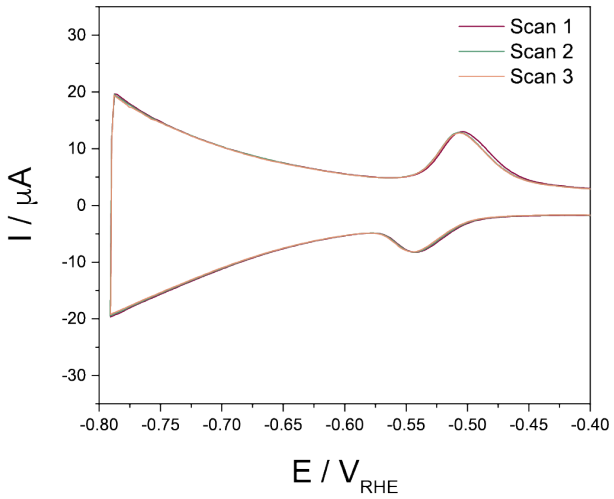

Figure S8. Subsequent SWV cycles of Ga NPs in CO_2-saturated 0.1 M $KHCO_3$ in the selected potentials range.

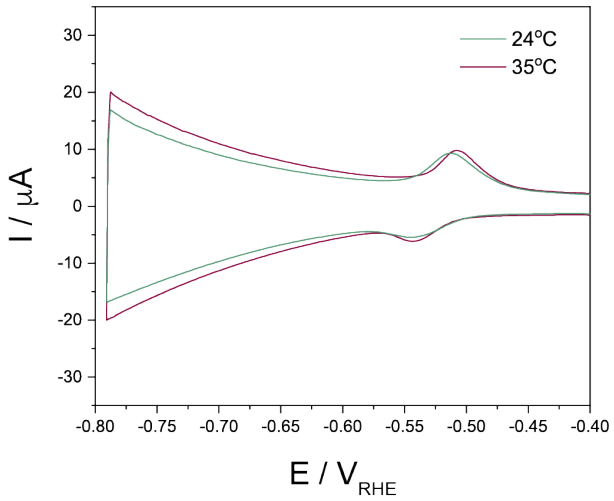

Figure S9. SWV of Ga NPs in CO_2-saturated 0.1 M $KHCO_3$ measured at 24 °C (below bulk Ga melting point, green line) and 35 °C (above bulk Ga melting point, red line).

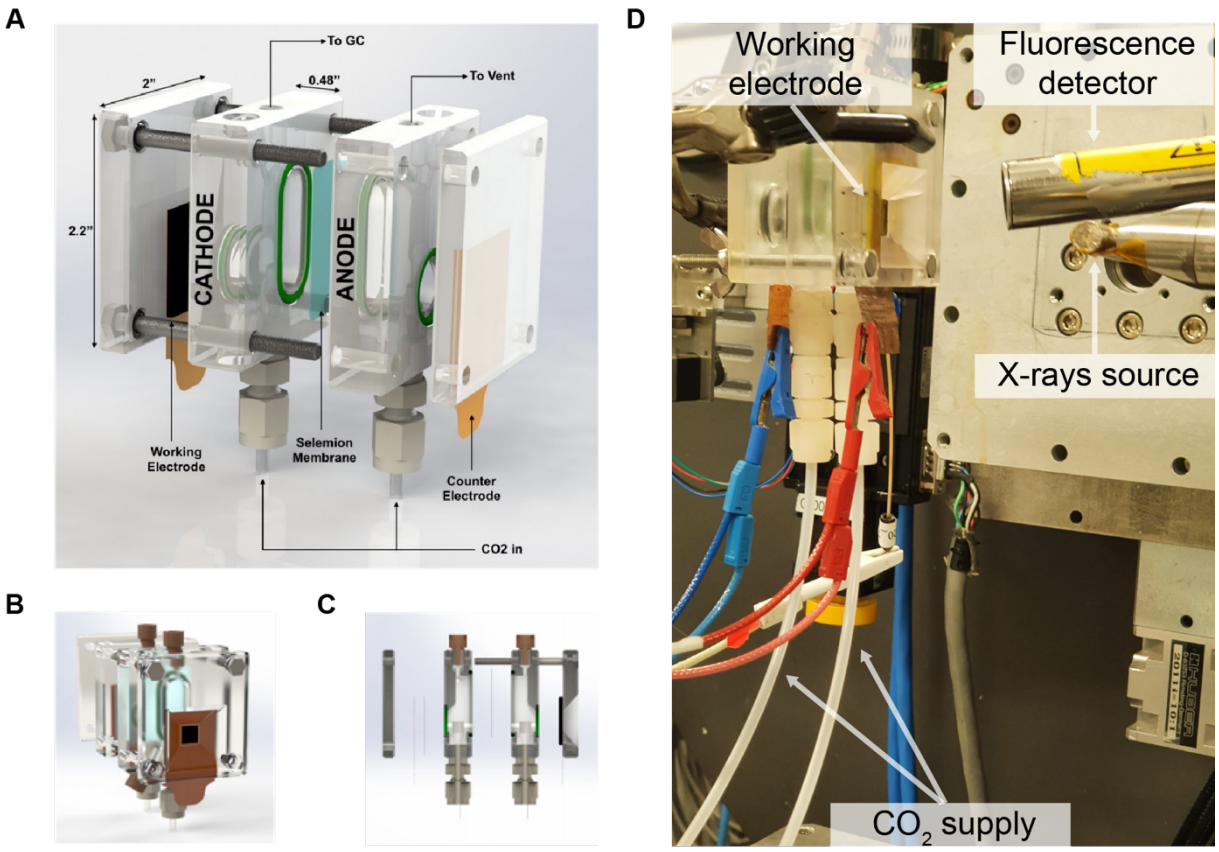

Figure S10. (A) Model of H-cell used in the measurements performed in the lab, reproduced from Iyengar *et al.*[11] (B) Face-view and (C) side-view of the cell used in *operando* XAS measurements, reproduced from Vavra et al.[12] (D) Photo of the experimental setup used in *operando* XAS measurements.

Ga oxide content calculation based on *operando* XAS measurements. *Operando* XAS is a bulk technique. As the linear fitting of oxide and metallic Ga components yields bulk ratio of these two components, we can use the data to obtain the thickness of Ga oxide layer (assuming all oxide is at the particle surface).

The total particle volume (V_p, nm^3) is obtained as the sum of metallic core (V_{met}, nm^3) and oxide shell (V_{ox}, nm^3):

$$V_p = V_{met} + V_{ox}$$

On the other hand, V_p and V_{met} can be calculated according to common equations for the volume of the sphere:

$$V_p = \frac{1}{6}\pi d_p^3 \quad V_{met} = \frac{1}{6}\pi d_{met}^3,$$

where $d_p = 26.2$ nm is the initial size diameter, d_{met} is the diameter of the metallic core.

From the linear fitting of the *operando* XAS measurements, we can obtain ω_{met}, which is the mass fraction of metallic Ga in the particle:

$$V_{met} = \omega_{met} V_p$$

This allows to obtain d_{met}:

$$d_{met} = \sqrt[3]{\frac{6}{\pi}V_{met}} = \sqrt[3]{\frac{6}{\pi}\omega_{met}V_p} = \sqrt[3]{\frac{6}{\pi}\omega_{met}\frac{1}{6}\pi d_p^3} = d_p\sqrt[3]{\omega_{met}}$$

Finally, if we define r_{ox} (nm) as oxide thickness, and considering that $d_p = d_{met} + 2r_{ox}$, we obtain the oxide thickness according to the following resulting equation:

$$r_{ox} = \frac{d_p - d_{met}}{2} = \frac{d_p - d_p\sqrt[3]{\omega_{met}}}{2} = \frac{d_p}{2}\left(1 - \sqrt[3]{\omega_{met}}\right), \text{ or}$$

$$r_{ox} = r_p\left(1 - \sqrt[3]{\omega_{met}}\right),$$

where $r_p = 13.1$ nm is the particle radius.

With the fitting results indicating that $\omega_{met}^{ocp} = 0.76$ and $\omega_{met}^{electrolysis} = 0.97$, we obtain $r_{ox}^{ocp} = 1.1$ nm and $r_{ox}^{electrolysis} = 0.13$ nm. Increase in particles size would concomitantly result in linear increase of the oxide thickness; with average particles size of 40 nm (**Figure S5**), we can expect that $r_{ox}^{electrolysis}$ may reach average value of 0.20 nm.

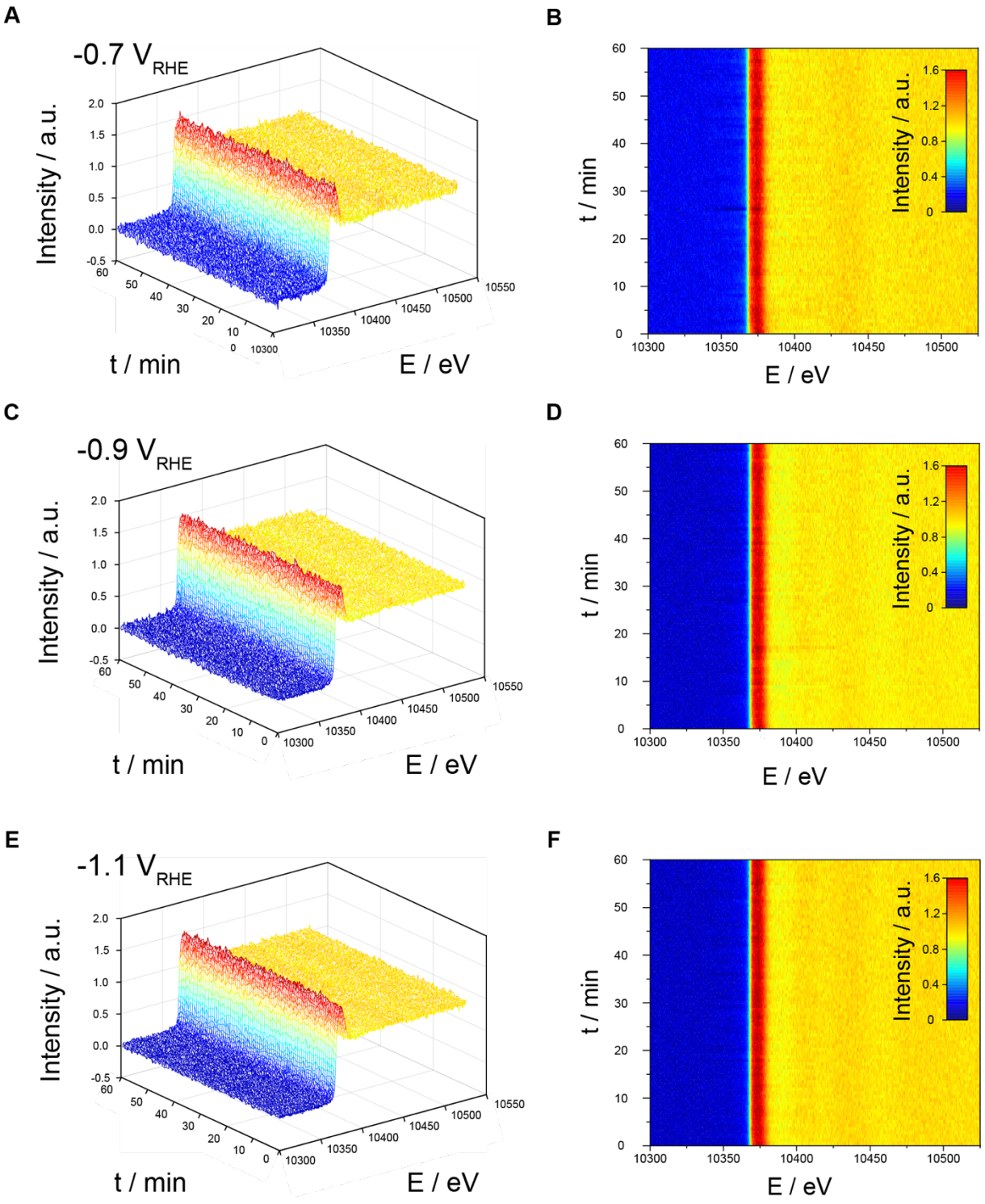

Figure S11. *Operando* XANES spectra of Ga NPs during 1 h CO_2RR at (A, B) -0.7 V_{RHE}, (C, D) -0.9 V_{RHE} and (E, F) -1.1 V_{RHE}: (A, C, E) 3D maps in time – voltage – intensity coordinates and (B, D, F) corresponding 2D maps in time – voltage coordinates. The white arrow indicates initial shift of the Ga K-edge absorption white line.

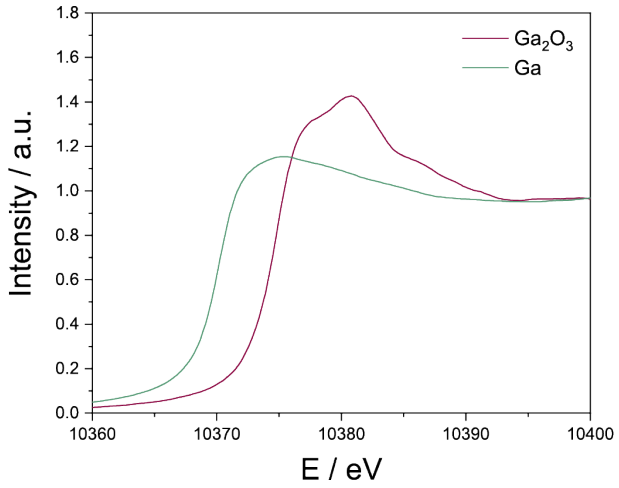

Figure S12. Reference XANES spectra of bulk Ga_2O_3 and metallic Ga.

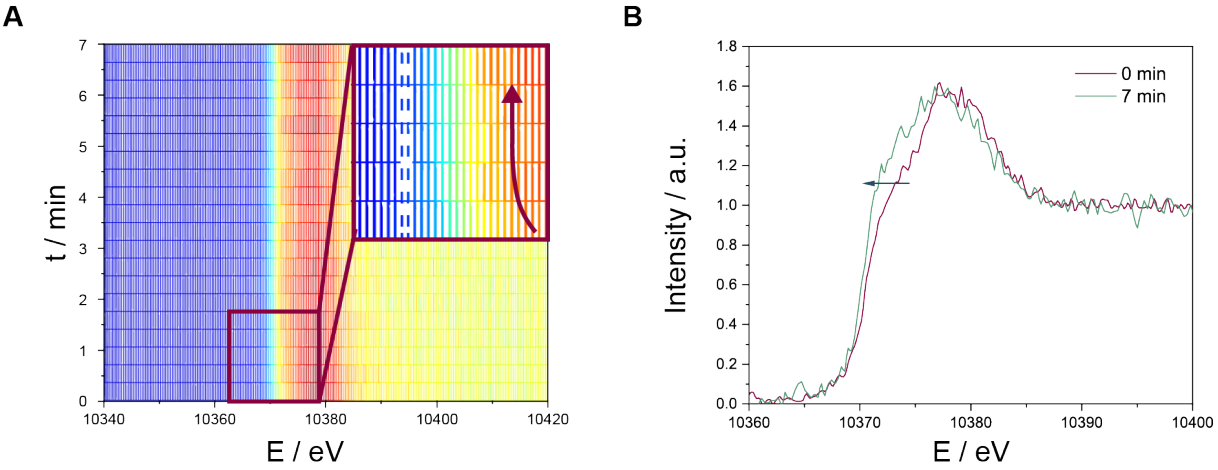

Figure S13. (A) *Operando* XANES obtained with 20 s scan duration and (B) comparison of the *operando* XANES scans at the start and after 7 min of electrolysis, showing shift of Ga K-edge absorption energy to lower values. This points at the reduction of Ga oxide majority during the first minutes of operation.

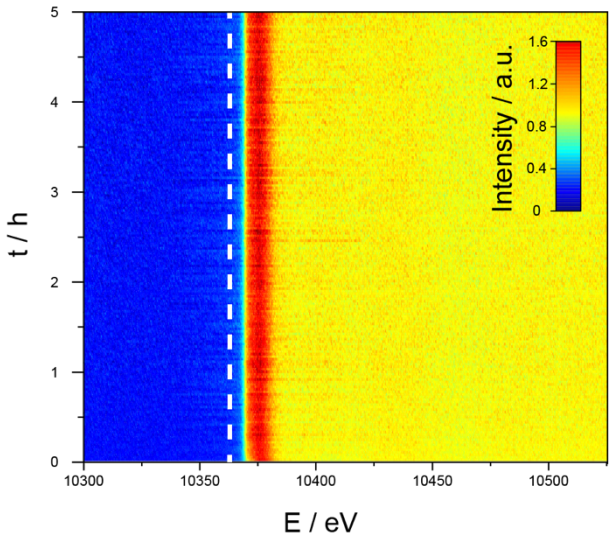

Figure S14. 2D map of the *operando* XANES spectra of Ga NPs during 5 h CO_2RR at -1.1 V_{RHE}.

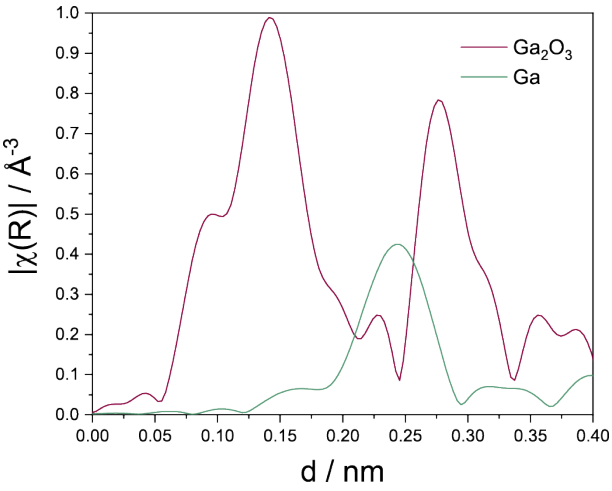

Figure S15. Interatomic distances derived from *operando* EXAFS measurements of Ga NPs at OCP and at -1.1 V_{RHE}. Interatomic distances were not corrected for the phase shift.

Ga electroreduction concept, CO_2RR and stoichiometry. The proposed mechanism of GaO_x reduction and formation happening simultaneously with CO_2RR does not affect total FE because the overall number of electrons transferred is balanced.

Indeed, the Ga reduction step consumes 3 electrons per 1 atom of Ga:

$$\frac{1}{2}Ga_2O_3 + 3e^- + \frac{3}{2}H_2O \rightarrow Ga^0 + 3OH^- \ (*)$$

We will further use Ga_2O_3 as surface state to simplify equations balancing; actual surface composition may vary, but it will not affect stoichiometry in a broad sense.

Then, according to the **Figure 7B**, Ga^0 surface reacts with protons from water with oxyhydroxide formation and reduction back to its metallic state driven by applied negative voltage:

$$Ga^0 + \frac{3}{2}H_2O \rightarrow \frac{1}{2}Ga_2O_3 + \frac{3}{2}H_2 \ (\text{B.1})$$

$$\frac{1}{2}Ga_2O_3 + 3e^- + \frac{3}{2}H_2O \rightarrow Ga^0 + 3OH^- \ (identical\ to\ *)$$

This way, 3/2 molecules of H_2 are formed by chemical reaction between Ga and water; however, the electron balance is conserved because the same number of electrons as would be needed to produce 3/2 H_2 are then consumed by Ga_2O_3 electroreduction. As (B.1) and (*) would follow each other over the course of electrolysis, overall electron balance is fulfilled.

On the other hand, considering that current increase and catalysis are observed only at voltages more cathodic that reduction peak (**Figure S3**), we assume CO_2 reduction happens on metallic Ga surface during the time when it is available (i.e., after reaction (*) and before reaction (B.1) takes place), with possible hydrogen evolution reaction as a competing process:

$$CO_{2_{ads}} + H_2O + 2e^- \rightarrow CO + 2OH^- \ (\text{B.2})$$

$$H_2O + e^- \rightarrow \frac{1}{2}H_2 + OH^- \ (\text{B.2}')$$

For both processes (B.2) and (B.2'), the charges transferred over the course of reactions are balanced: the electrons supplied from the cathode are transferred directly to reagents (CO_2 and H_2O). It means that, overall, mechanism presented at **Figure 7B** would not result in total FE misrepresentation.

The mechanism presented on **Figure 7C** implies that, contrary to the previous case, it is Ga which reduces CO_2 directly:

$$Ga^0 + \frac{3}{2}CO_2 \rightarrow \frac{1}{2}Ga_2O_3 + \frac{3}{2}CO \ (\mathrm{C}.1)$$

Depending on the exact oxide skin stoichiometry and hydrolyzation extent, H_2 can be also produced as a by-product, e.g., according to the following equation:

$$Ga^0 + CO_2 + H_2O \rightarrow GaOOH + CO + \frac{1}{2}H_2 \ (\mathrm{C}.1')$$

As a result, CO/H_2 mixture of varied composition is formed here. In any case, formation of the resulting gas mixture requires transfer of 3 electrons from Ga, which are than consumed during reduction of Ga_2O_3 in the next step where metallic Ga surface is recovered:

$$\frac{1}{2}Ga_2O_3 + 3e^- + \frac{3}{2}H_2O \rightarrow Ga^0 + 3OH^- \ (identical\ to\ *)$$

Overall, any mechanism does not in total FE misevaluation, as total electron balance is fulfilled despite differences in the nature of the processes involved. Moreover, even if we assume formation of unstable Ga(I) species, the total FE values which we obtain will remain valid thanks to the charges balance condition which will remain fulfilled.

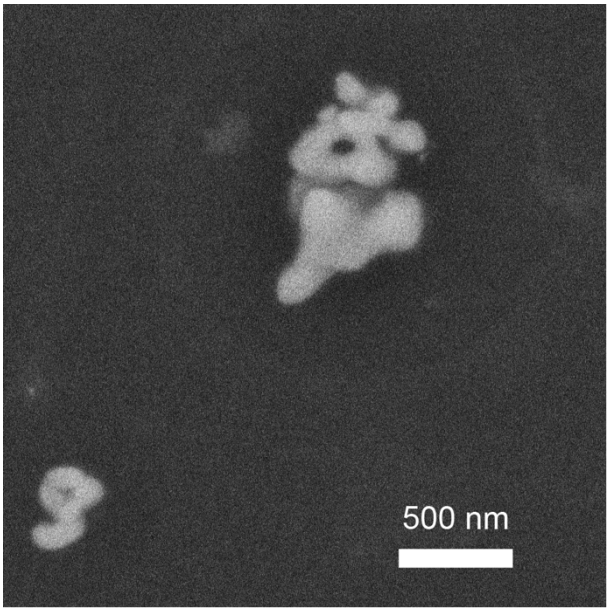

Figure S16. SEM image of Ga NPs electrode after 10 min immersion in 1 M HCl.

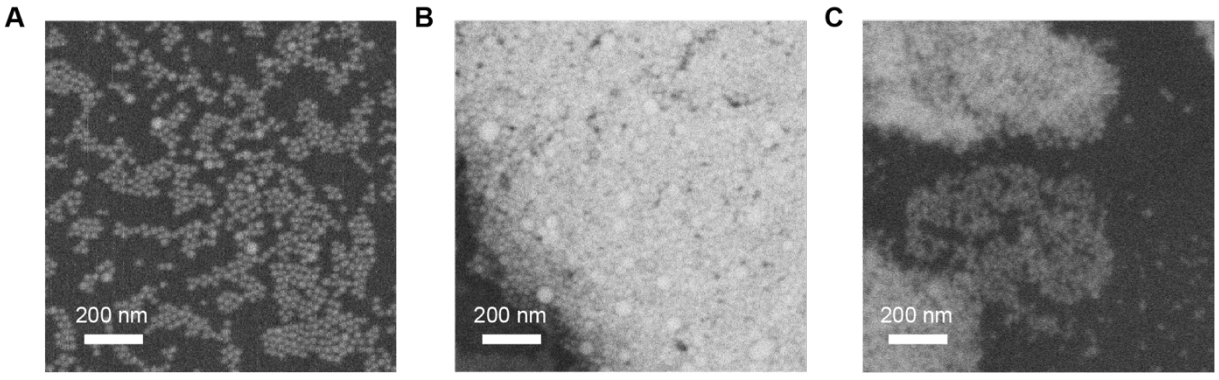

Figure S17. SEM images of Ga NPs electrodes after electrolysis at -0.7 V_{RHE} in (A) 0.1 M phosphate buffer (pH = 6.8) under CO_2 flow, (B) 0.1 M $KHCO_3$ under N_2 flow and (C) 0.1 M phosphate buffer (pH = 6.8) under N_2 flow.

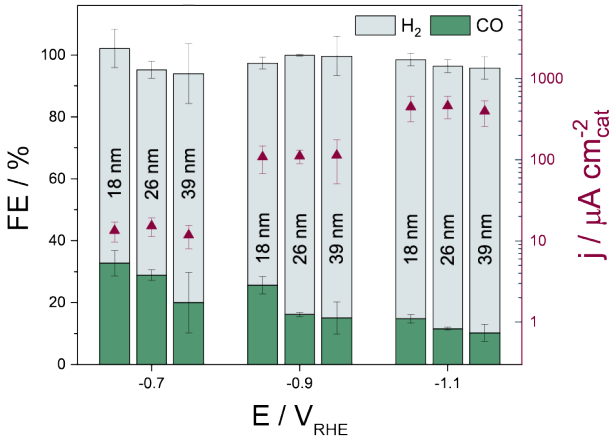

Figure S18. SEM images of 18 nm, 26 nm and 39 nm Ga NPs electrodes before and after electrolysis at -0.7 V_{RHE}, -0.9 V_{RHE} -1.1 V_{RHE}.

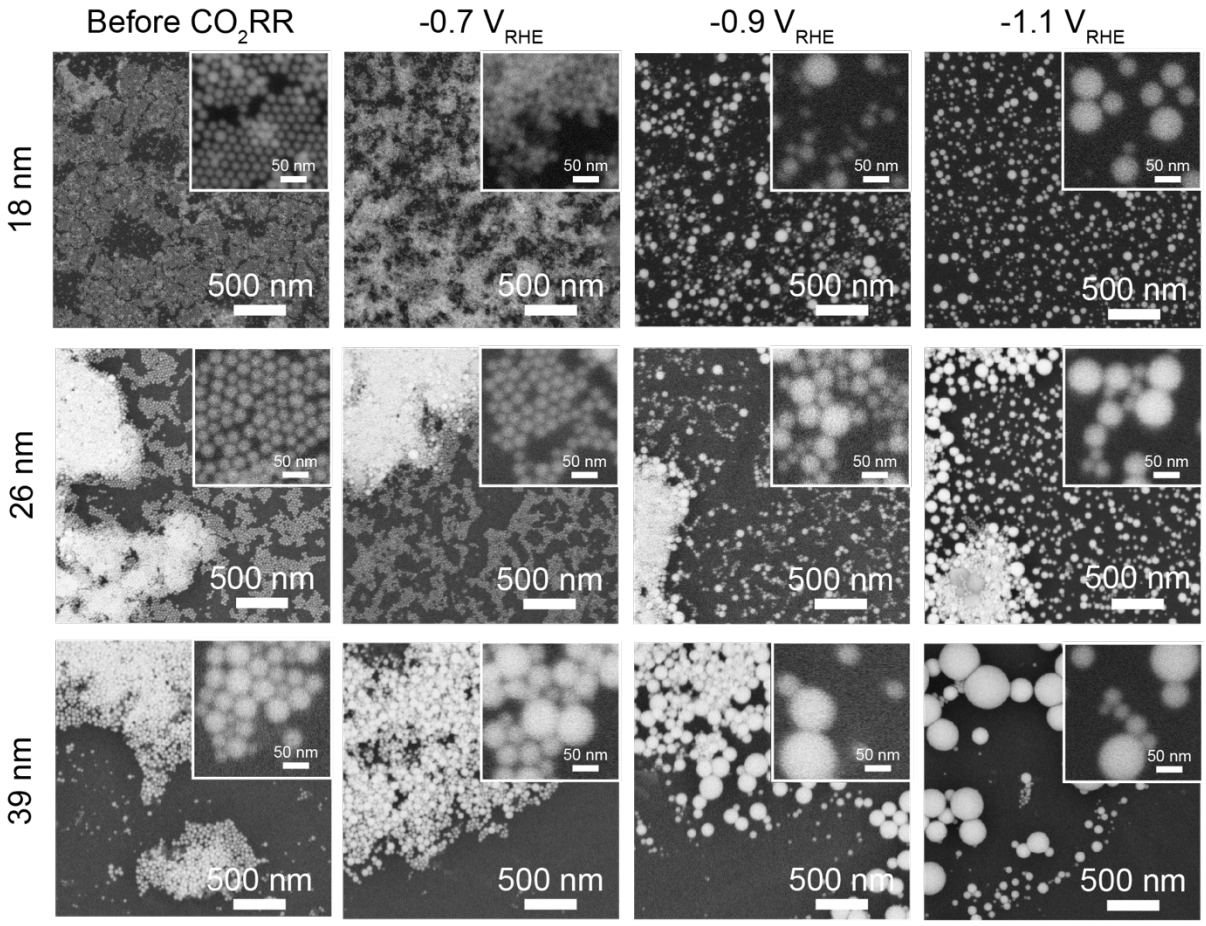

Figure S19. SEM images of 18 nm, 26 nm and 39 nm Ga NPs electrodes before and after electrolysis at -0.7 V_{RHE}, -0.9 V_{RHE} -1.1 V_{RHE}.

Given the *ex situ* nature of the SEM analysis, the possibility that the Ga NPs coalesce into bulk film at negative voltage and fragment back when oxide skin is restored upon exposure to air exist. However, as Ga NPs loading is identical in all cases, bulk film fragmentation would yield similar post-SEM particles size distribution. This hypothesis was discarded by testing particles of different sizes (**Figure S20**).

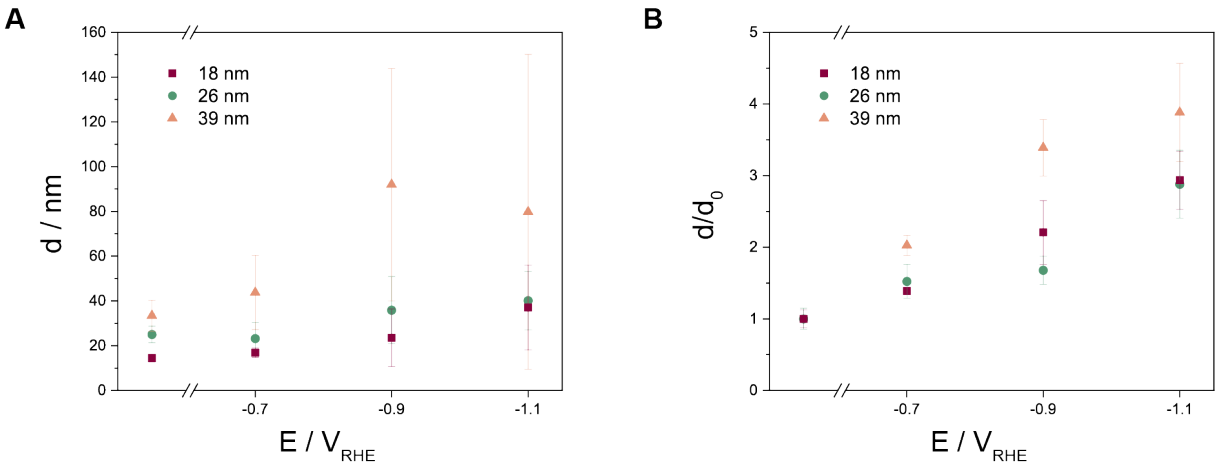

Figure S20. Statistical analysis performed on SEM images of 18 nm, 26 nm and 39 nm Ga NPs electrodes after electrolysis at -0.7 V_{RHE}, -0.9 V_{RHE} -1.1 V_{RHE}. The analysis is based on (A) average particles size and (B) ratio between the average size of coalesced particles vs. initial size of Ga NPs. The first points refer to the size of Ga NPs on the as-prepared electrodes.

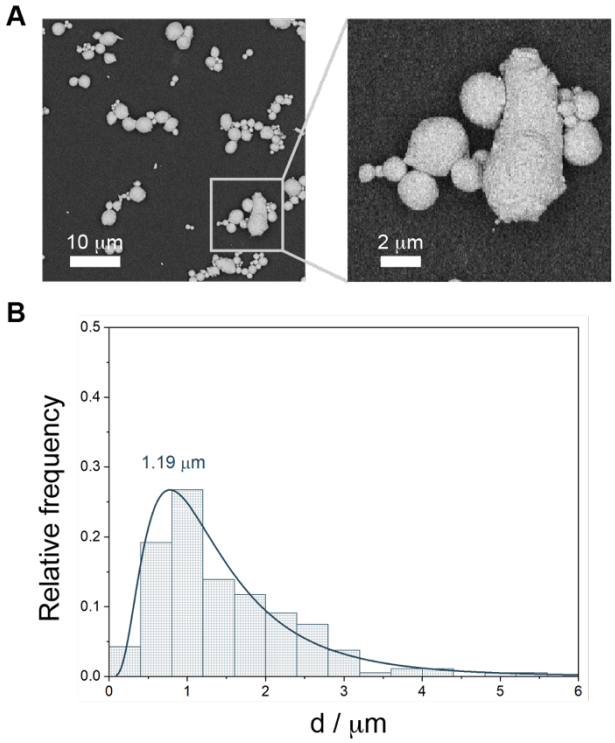

Figure S21. (A) SEM images and (B) size distribution of Ga MPs.

References

(1) He, M.; Protesescu, L.; Caputo, R.; Krumeich, F.; Kovalenko, M. V. A General Synthesis Strategy for Monodisperse Metallic and Metalloid Nanoparticles (In, Ga, Bi, Sb, Zn, Cu, Sn, and Their Alloys) via *In situ* Formed Metal Long-Chain Amides. *Chem. Mater.* **2015**, *27*, 635–647.

(2) Falchevskaya, A. S.; Prilepskii, A. Y.; Tsvetikova, S. A.; Koshel, E. I.; Vinogradov, V. V. Facile Synthesis of a Library of Hollow Metallic Particles through the Galvanic Replacement of Liquid Gallium. *Chem. Mater.* **2021**, *33*, 1571–1580.

(3) Batchellor, A. S.; Boettcher, S. W. Pulse-Electrodeposited Ni-Fe (Oxy)Hydroxide Oxygen Evolution Electrocatalysts with High Geometric and Intrinsic Activities at Large Mass Loadings. *ACS Catal.* **2015**, *5*, 6680–6689.

(4) Doyle, R. L.; Lyons, M. E. G. An Electrochemical Impedance Study of the Oxygen Evolution Reaction at Hydrous Iron Oxide in Base. *Phys. Chem. Chem. Phys.* **2013**, *15*, 5224–5237.

(5) Lyons, M. E. G.; Brandon, M. P. The Significance of Electrochemical Impedance Spectra Recorded during Active Oxygen Evolution for Oxide Covered Ni, Co and Fe Electrodes in Alkaline Solution. *J. Electroanal. Chem.* **2009**, *631*, 62–70.

(6) Moysiadou, A.; Lee, S.; Hsu, C. S.; Chen, H. M.; Hu, X. Mechanism of Oxygen Evolution Catalyzed by Cobalt Oxyhydroxide: Cobalt Superoxide Species as a Key Intermediate and Dioxygen Release as a Rate-Determining Step. *J. Am. Chem. Soc.* **2020**, *142*, 11901–11914.

(7) Reske, R.; Mistry, H.; Behafarid, F.; Roldan Cuenya, B.; Strasser, P. Particle Size Effects in the Catalytic Electroreduction of CO_2 on Cu Nanoparticles. *J. Am. Chem. Soc.* **2014**, *136*, 6978–6986.

(8) Cicco, A. Di. Phase Transitions in Confined Gallium Droplets. *Phys. Rev. Lett.* **1998**, *81*, 2942.

(9) Yarema, M.; Wörle, M.; Rossell, M. D.; Erni, R.; Caputo, R.; Protesescu, L.; Kravchyk, K. V.; Dirin, D. N.; Lienau, K.; Von Rohr, F.; Schilling, A.; Nachtegaal, M.; Kovalenko, M. V. Monodisperse Colloidal Gallium Nanoparticles: Synthesis, Low Temperature Crystallization, Surface Plasmon Resonance and Li-Ion Storage. *J. Am. Chem. Soc.* **2014**, *136*, 12422–12430.

(10) Castilla-Amorós, L.; Chien, T. C. C.; Pankhurst, J. R.; Buonsanti, R. Modulating the Reactivity of Liquid Ga Nanoparticle Inks by Modifying Their Surface Chemistry. *J. Am. Chem. Soc.* **2022**, *144*, 1993–2001.

(11) Iyengar, P.; Huang, J.; De Gregorio, G. L.; Gadiyar, C.; Buonsanti, R. Size Dependent Selectivity of Cu Nano-Octahedra Catalysts for the Electrochemical Reduction of CO_2 to CH_4. *Chem. Commun.* **2019**, *55*, 8796–8799.

(12) Vavra, J.; Shen, T.-H.; Stoian, D.; Tileli, V.; Buonsanti, R. Real-time Monitoring Reveals Dissolution/Redeposition Mechanism in Cu Nanocatalysts during the Initial Stages of the CO_2 Reduction Reaction. *Angew. Chemie Int. Ed.* **2021**, *60*, 1347–1354.